THE BUCKLING AND POSTBUCKLING BEHAVIOUR OF CURVED CFRP LAMINATED SHEAR PANELS

ICAS-88-5.6.3

K. Wolf and H. Kossira

Institute for Aircraft Design and Structural Mechanics
Technical University Braunschweig, FR Germany

Abstract

Results of a theoretical and experimental study on the buckling and postbuckling behaviour of curved carbon fibre reinforced plastic (CFPR) panels subjected to shear loading are presented. The theoretical investigations were performed using a newly developed nonlinear finite element computer program. This program is capable of calculating linear buckling loads and nonlinear postbuckling behaviour including snap-through and material failure. Numerical results are presented showing the effect of curvature, boundary conditions and initial geometric imperfections on the buckling and postbuckling behaviour. To verify the applied numerical method additional tests were carried out. The experimental results were compared with theoretical predictions. The comparison revealed a reasonably good correlation between theory and experiment.

1. Introduction

Weight saving is one of the most important requirements in aircraft and spacecraft structural design. One way to reduce structural weight is the use of new high strength lightweight materials like carbon fibre reinforced plastics (CFRP). In the case of thinwalled primary structures further weight savings can be obtained using their postbuckling strength. Typical examples are shear loaded fuselage panels which have a considerable load bearing capacity in the postbuckling range. Essential requirements for the utilization of existing postbuckling strength are the understanding of the instability phenomenons and informations about the limit load. Thus, theoretical investigations are necessary taking into account the effects of large deformation and material failure.

The buckling and postbuckling behaviour of curved composite panels under compression and of composite plates under shear load has been examined in a considerable number of publications (e.g. references [1,2,3]), whereas only few papers relate to curved shear panels. Most of them deal with the analysis of the linear buckling load (e.g. ref. [4]). Only one theoretical study of the postbuckling behaviour has been presented so far [5]. In this paper HUI and DU examined the initial postbuckling behaviour and the imperfection-sensitivity of infinitly long cylindrical composite panels. Experimental investigations were conducted by WILKINS and OLSON [6]. A CFRP-cylinder consisting of four curved panels was tested. The load was applied by torsion. As the collaps load of the panels exceeded only slightly the buckling load, no informations about the behaviour in the deep postbuckling range were obtained. Theoretical studies on shear panels considering material failure in the postbuckling range are not known.

The objective of this paper is to examine the buckling and postbuckling behaviour of cylindrical CFRP panels subjected to shear loading both theoretically and experimentally. A numerical method based on a mixed finite element model is presented. It is capable of calculating a nonlinear load-deformation path in the postbuckling range including bifurcation and snap-through, detecting material failure, analysing the damage accumulation, and determining the collapse load. As examples, a series of computations have been carried out for curved panels having different curvature, different initial imperfections, and different boundary conditions. In addition, results of experimental investigations are presented and compared with theoretical predictions.

2. Theoretical Study

Numerical method

In this study the buckling and postbuckling analysis of laminated panels (see Fig.1) is based on a nonlinear shell theory of the Kirchhoff-Love type [7]. The applied theory is valid for thin deep shells subjected to large deformations but only moderate rotations. A total Lagrangian formulation is used i.e., the state of the deformed panel is expressed in terms of the initial state. The nonlinear differential equations of the shell theory are transformed into a set of algebraic equations by means of the finite element method (FEM)[8]. A mixed variational principle[9] is used to derive a cylindrical shell element. The major advantage of the used principle is that simple structured element matrices are obtained and only C^0-continuity is required [7].

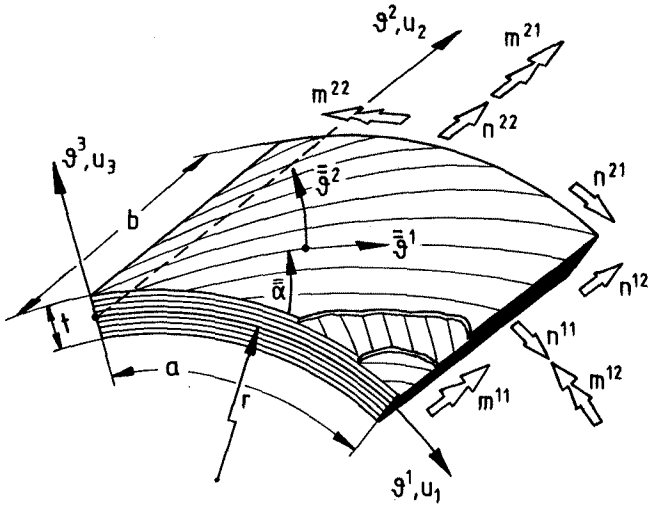

Figure 1. Cylindrical panel: geometry, displacements, resultant stresses and moments.

For a deformed cylindrical panel the mixed principle reads

$$\delta A = \delta \int_F \left(\underline{\sigma}^T \underline{\gamma} - \frac{1}{2} \underline{\sigma}^T \underline{C}^{-1} \underline{\sigma} \right) dF - \int_F \delta \underline{u}^T \underline{\bar{p}} \, dF = 0 \qquad (1)$$

with the vectors

$$\underline{\sigma} = \begin{bmatrix} n^{\alpha\beta} \\ m^{\alpha\beta} \end{bmatrix}, \quad \underline{\gamma} = \begin{bmatrix} \alpha_{\alpha\beta} \\ \beta^*_{\alpha\beta} \end{bmatrix}, \quad \underline{u} = \begin{bmatrix} u_i \end{bmatrix}, \quad \underline{\bar{p}} = \begin{bmatrix} p^i \end{bmatrix}$$

and the matrix

$$\underline{C} = \left[\begin{array}{c|c} C_D^{\alpha\beta\varrho\lambda} & C_K^{\alpha\beta\varrho\lambda} \\ \hline C_K^{\alpha\beta\varrho\lambda} & C_B^{\alpha\beta\varrho\lambda} \end{array}\right]$$

containing the material properties. The indices $\alpha,\beta,\varrho,\lambda$ running from 1 to 2 and i running from 1 to 3 indicate the direction of the mechanical vector quantities (see Fig.1). δA is the virtual work and F the middle surface of the undeformed panel. The vector $\underline{u}$ contains the displacements u_i of the middle surface and $\underline{\bar{p}}$ the the conservative external loads p^i. The state of stress in the panel is defined by the in-plane stress resultants $n^{\alpha\beta}$ and the moments $m^{\alpha\beta}$ [10]. They are Piola-Kirchhoff quantities of the 2. kind. The relationship between strains and displacements is defined by the nonlinear operator matrix $\underline{D}$:

$$\underline{\gamma} = \underline{D}\,\underline{u} = \left(\underline{D}_L + \underline{D}_N\right)\underline{u} \rightarrow \begin{bmatrix} \alpha_{\alpha\beta} \\ \beta^*_{\alpha\beta} \end{bmatrix} = \begin{bmatrix} \underline{D}_L^D + \underline{D}_N^D \\ \underline{D}_L^B \end{bmatrix} \underline{u} \qquad (2)$$

with

$$\underline{D}_L^B = \left[\begin{array}{c|c|c} -{}_1\partial\frac{2}{r} & 0 & {}_1\partial\partial_1 + \frac{1}{r^2} \\ \hline 0 & 0 & {}_2\partial\partial_2 \\ \hline -{}_2\partial\frac{2}{r} & 0 & {}_2\partial\partial_1 + {}_1\partial\partial_2 \end{array}\right],$$

$$\underline{D}_L^D = \left[\begin{array}{c|c|c} \partial_1 & 0 & \frac{1}{r} \\ \hline 0 & \partial_2 & 0 \\ \hline \partial_2 & \partial_1 & 0 \end{array}\right],$$

$$\underline{D}_N^D = \frac{1}{2}\left[\begin{array}{c|c|c} \frac{1}{r^2}u_1 + u_{1,1}\partial_1 & u_{2,1}\partial_1 & \frac{1}{r}(u_{1,1} - u_1\partial_1) \\ -\frac{1}{r}(u_{3,1} - u_3\partial_1) & & +\frac{1}{r^2}u_3 + u_{3,1}\partial_1 \\ \hline u_{1,2}\partial_2 & u_{2,2}\partial_2 & u_{3,2}\partial_2 \\ \hline u_{1,1}\partial_2 + u_{1,2}\partial_1 & u_{2,1}\partial_2 & \frac{1}{r}(u_{1,2} - u_1\partial_2) \\ -\frac{1}{r}(u_{3,2} - u_{3,2}\partial_2) & +u_{2,2}\partial_1 & +u_{3,1}\partial_2 + u_{3,2}\partial_1 \end{array}\right].$$

∂_α indicates differentiation with respect to ϑ^α. $\alpha_{\alpha\beta}$ are the membran strains and $\beta^*_{\alpha\beta}$ the flexural curvatures. The operators $\underline{D}_L$ and $\underline{D}_N$ are valid for large deformations with moderate rotations of the normals to the middle surface. The matrix $\underline{C}$ contains the stiffness properties of a general laminate. The inplane, coupling, and bending stiffnesses $C_D^{\alpha\beta\varrho\lambda}$, $C_K^{\alpha\beta\varrho\lambda}$, and $C_B^{\alpha\beta\varrho\lambda}$ are determined using the classical laminate theory [11]

$$\left[C_D^{\alpha\beta\varrho\lambda};\, C_K^{\alpha\beta\varrho\lambda};\, C_B^{\alpha\beta\varrho\lambda}\right] = \int_{-\frac{t}{2}}^{\frac{t}{2}} E_m^{\alpha\beta\varrho\lambda}\left[1;\, \vartheta^3;\, (\vartheta^3)^2\right] d\vartheta^3. \qquad (3)$$

$E_m^{\alpha\beta\varrho\lambda}$ are the moduli of the single layer "m". They depend upon the type of material and the fibre orientation $\bar{\alpha}$. In case of nonlinear material properties (e.g. lamina failure), $E_m^{\alpha\beta\varrho\lambda}$ and $\underline{C}$ are also functions of the lamina stresses and strains.

Using the strain-displacement relations (2), the strains in equation (1) are substituted by the displacements:

$$\delta A = \delta \int_F \left(\underline{\sigma}^T \underline{D}\,\underline{u} - \frac{1}{2} \underline{\sigma}^T \underline{C}^{-1} \underline{\sigma} \right) dF - \int_F \delta \underline{u}^T \underline{\bar{p}} \, dF = 0 \,. \qquad (4)$$

Now the mixed variational principle has the stress resultants $n^{\alpha\beta}$, the moments $m^{\alpha\beta}$, and the displacements u_i of the middle surface as unknown variables.

As the problem described by equation (4) is highly nonlinear and pathdependend, an incremental solution strategy is required. In order to obtain an incremental formulation, two different states of deformation are introduced. In the fundamental state, denoted by the index ι, the static and kinematic variables of the deformed panel are known. Applying a load increment $\Delta\underline{\bar{p}}$ the adjacent state (index $\iota+1$) is obtained. The variables of the adjacent state can be expressed as

$$\begin{aligned} {}^{\iota+1}\underline{\sigma} &= {}^{\iota}\underline{\sigma} + \Delta\underline{\sigma} \\ {}^{\iota+1}\underline{u} &= {}^{\iota}\underline{u} + \Delta\underline{u} \end{aligned} \qquad (5)$$

with the unknown increments $\Delta\underline{\sigma}$ and $\Delta\underline{u}$.

Substituting equation (5) in (4) the incremental virtual work

$$\delta\Delta A = \delta^{l+1}A - \delta^{l}A \qquad (6)$$

is obtained. Transformed in a symmetric matrix form the incremental mixed variational principle reads

$$\delta\Delta A = \int_F \delta\Delta\underline{z}^T \left(\underline{A}_E + \underline{A}_P + \underline{A}_G\right)\Delta\underline{z}\, dF - \int_F \delta\Delta\underline{z}^T \Delta\underline{p}\, dF = 0 \qquad (7)$$

with

$$\Delta\underline{z} = \begin{bmatrix} \Delta\underline{u} \\ \Delta\underline{q} \end{bmatrix} \; ; \quad \Delta\underline{p} = \begin{bmatrix} \Delta\bar{\underline{p}} \\ \underline{0} \end{bmatrix}.$$

The operator matrix $\underline{A}_E$ represents the linear elastic virtual work and $\underline{A}_P$ the influence of material nonlinearities. The geometric nonlinear operator $\underline{A}_G$ contains nonlinear terms of the stresses ${}^{l}\underline{q}$ and displacements ${}^{l}\underline{u}$ of the fundamental state.

In order to obtain a set of algebraic equations from (7), the panel is divided into finite shell elements. For an arbitrary element (e) the incremental variables $\Delta\underline{z}$ are approximated by

$$\Delta\underline{z}^{(e)} = \underline{\Phi}\,\Delta\hat{\underline{z}}^{(e)} \qquad (8)$$

where $\underline{\Phi}$ contains interpolation functions and $\Delta\hat{\underline{z}}^{(e)}$ the kinematic and static variables of the nodal points. As the operators in (7) contain only first order derivatives with respect to the coordinates ϑ^{α}, linear interpolation functions were chosen. In order to prevent numerical defects (e.g. locking, oscillating solutions) the functions were modified. The obtained element has 4 nodes, each with 9 degrees of freedom

$$\Delta\hat{\underline{z}}^{(e)} = \Delta\left[\hat{u}_1, \hat{u}_2, \hat{u}_3, \hat{n}^{11}, \hat{n}^{22}, \hat{n}^{12}, \hat{m}^{11}, \hat{m}^{22}, \hat{m}^{12}\right]^T_{(e)} . \qquad (9)$$

The substitution of the approximation (8) into (7) leads to the following set of linear algebraic equations valid for a single element

$$\left[\underline{K}_E^{(e)} + \underline{K}_P^{(e)} + \underline{K}_G^{(e)}\left({}^{l}\hat{\underline{z}}^{(e)}\right)\right]\Delta\hat{\underline{z}}^{(e)} = \Delta\hat{\underline{p}}^{(e)} \qquad (10)$$

with

$$\underline{K}_i^{(e)} = \int_F \underline{\Phi}^T \underline{A}_i^{(e)} \underline{\Phi}\, dF \qquad i = E,P,G$$

$$\Delta\hat{\underline{p}}^{(e)} = \int_F \underline{\Phi}^T \Delta\underline{p}^{(e)}\, dF .$$

A subsequent element assemblage process creates the global matrices and vectors of the complete panel

$$\underline{K}_{E,P,G} = \sum_{(e)} \underline{K}_{E,P,G}^{(e)} \; ; \quad \Delta\hat{\underline{z}} = \sum_{(e)} \Delta\hat{\underline{z}}^{(e)} \; ; \quad \Delta\hat{\underline{p}} = \sum_{(e)} \Delta\hat{\underline{p}}^{(e)} \qquad (11)$$

and leads to the linearized system of algebraic equations for a load increment

$$\left[\underline{K}_E + \underline{K}_P + \underline{K}_G\left({}^{l}\hat{\underline{z}}\right)\right]\Delta\hat{\underline{z}} = \underline{K}\left({}^{l}\hat{\underline{z}}\right) = \Delta\hat{\underline{p}} . \qquad (12)$$

$\underline{K}$ represents the tangent to the solution path at the fundamental state "l". Applying an incremental load step equation (12) yields a trial solution for the adjacent state "$l+1$"

$${}^{l+1}\hat{\underline{z}} = {}^{l}\hat{\underline{z}} + \Delta\hat{\underline{z}} . \qquad (13)$$

As the load increment is of finite size, linearization errors occur. These errors are corrected by an iterative solution procedure. Since standard solution procedures like the modified Newton-Raphson method are inefficient in the vicinity of critical points, an arc-length-method is used. This iteration technique allows to trace "snap-through" as well as "snap-back" behaviour [12,13].

To detect points of neutral equilibrum (bifurcation and limit points) during the computation of nonlinear solution paths, equation (13) has to be transformed in an eigenvalue problem. Provided that the kinematic and static variables of the fundamental state "l" depend linearly upon the applied external load they may be enlarged by a load factor λ:

$${}^{l}\hat{\underline{z}} \;\longrightarrow\; \lambda\,{}^{l}\hat{\underline{z}} . \qquad (14)$$

Using the static stability criterion together with (14), a linear eigenvalue problem is obtained from (13)[12]

$$\left[\underline{K}_E + \underline{K}_P + \lambda\underline{K}_G\left({}^{l}\hat{\underline{z}}\right)\right]\hat{\underline{z}} = 0 . \qquad (15)$$

The smallest eigenvalue $\lambda = \lambda_{cr}$ gives an approximation for the difference between the load level of the fundamental state and that of the nearest critical point. For $\lambda_{cr} = 1$ a critical point is reached. In case of a bifurcation point the eigenvector $\hat{\underline{z}}$ gives the eigenmode of the intersecting secondary solution path. To follow this secondary path, a fraction of the eigenmode is superimposed on the displacement field at the critical load.

To perform a "classical" linear buckling analysis, it has to be assumed that the panel is in an undeformed fundamental state ($l = 0$) with only membrane forces acting (${}^{l}\hat{\underline{z}} = {}^{0}\hat{\underline{z}} = {}^{0}\hat{\underline{n}}$). This leads to the linear eigenvalue problem [12]

$$\left[\underline{K}_E + \lambda\underline{K}_G\left({}^{0}\hat{\underline{n}}\right)\right]\hat{\underline{z}} = 0 . \qquad (16)$$

As stated before, material nonlinearities may be included in the numerical analysis. In the present study the analysis is limited to nonlinear material behaviour which follows from matrix and fibre failure of single laminas. For each load increment each lamina is checked at every nodal point using the following failure criteria:

Matrix failure [14]

$$\frac{\left(\bar{\bar{\sigma}}^{11}\right)^2}{\bar{\bar{\sigma}}^{11}_{FC}\,\bar{\bar{\sigma}}^{11}_{FT}} + \frac{\left(\bar{\bar{\sigma}}^{22}\right)^2}{\bar{\bar{\sigma}}^{22}_{FC}\,\bar{\bar{\sigma}}^{22}_{FT}} + \left(\frac{\bar{\bar{\sigma}}^{12}}{\bar{\bar{\sigma}}^{12}_{FT}}\right)^2 + \left(\frac{1}{\bar{\bar{\sigma}}^{11}_{FT}} - \frac{1}{\bar{\bar{\sigma}}^{11}_{FC}}\right)\bar{\bar{\sigma}}^{11} + \left(\frac{1}{\bar{\bar{\sigma}}^{22}_{FT}} - \frac{1}{\bar{\bar{\sigma}}^{22}_{FC}}\right)\bar{\bar{\sigma}}^{22} = 1$$

Fibre failure [14]

$$\left(\frac{\bar{\bar{\sigma}}^{11}}{\bar{\bar{\sigma}}^{11}_{FC,FT}} \right)^2 = 1 \ .$$

$\bar{\bar{\sigma}}^{11}, \bar{\bar{\sigma}}^{22}, \bar{\bar{\sigma}}^{12}$ are the current lamina stresses with respect to the lamina coordinate system. The index F denotes the failure stresses, T indicates tension and C compression. If a failure is detected, the lamina stiffness is reduced at the concerned nodal point according to the failure mode and the matrix K_P is updated. Details of the used procedure are reported in reference [13] .

The presented numerical strategies are incorporated in the finite element computer code FiPPS, which was developed at the IFL.

Theoretical results

Using the developed computational procedure theoretical studies were performed to examine the influence of curvature, boundary conditions and geometric imperfections on the buckling and postbuckling behaviour of CFRP shear panels. Some of the obtained results are presented.

The dimensions, the material properties and the finite element idealization (12x12 mesh) of the studied panels are shown in Figure 2. The shear load was applied by shearing the panel edges which are assumed to have infinite rigidity. For the idealization of deep panels (a/r > 0,2) a refined element mesh (16x16) was used. All computations were performed on an Amdahl 470 V/7 computer.

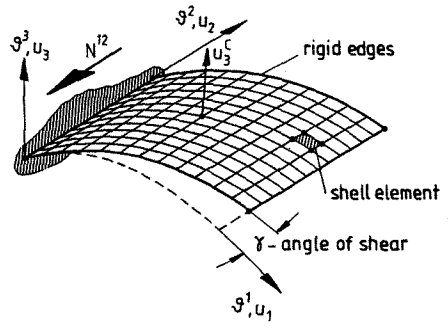

dimensions :	material :
a = b = 400 mm	lay-up $[\pm 45]_s$
t = 2,5 mm	E_1 = 139000 N/mm²
	E_2 = 8990 N/mm²
boundary cond. :	G_{12} = 4640 N/mm²
clamped	ν_{12} = 0,35 N/mm²

Figure 2. Data and FEM-idealization of the examined panels.

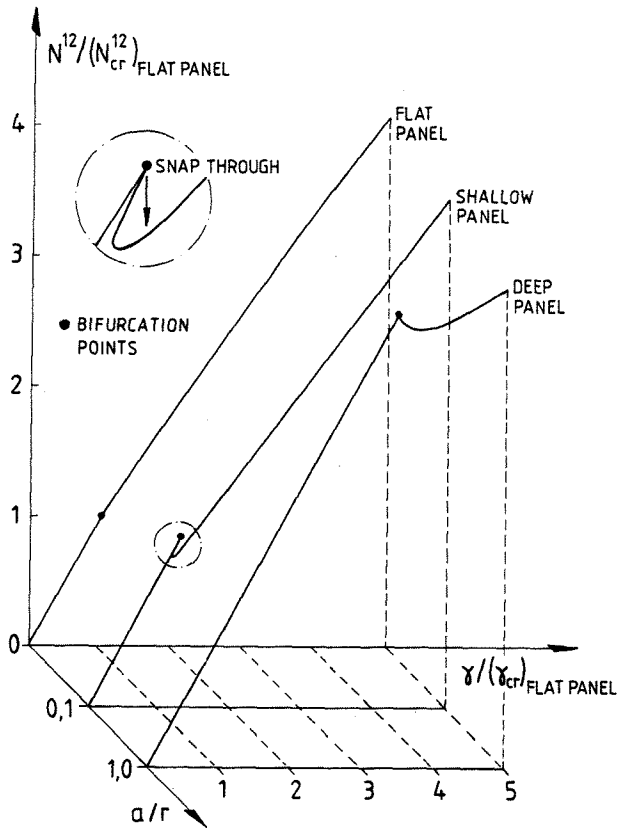

Figure 3. Effect of panel curvature on the relation between the average shear flow N^{12} and the angle of shear γ .

First, the influence of the panel curvature shall be examined. Figure 3 shows a graph of the average shear flow at the edge

$$N^{12} = \frac{1}{b} \int_0^b n^{12} \left(\vartheta^1 = 0 ; \vartheta^2 \right) d\vartheta^2$$

versus the prescribed angle of shear γ for a flat, a shallow and a deep panel. N^{12} and γ are normalized with respect to the corresponding values of the classical buckling load of the flat panel, denoted by the index cr . The gradient $dN^{12}/d\gamma$ may be interpreted as the global shear stiffness of the panels.

All panels show a linear prebuckling behaviour. The load level of the bifurcation points, located during the nonlinear computation, are identical with the classical buckling load. The bifurcation load increases with decreasing radius of curvature. The initial postbuckling behaviour of the three panels differs fundamentally. The N^{12}-γ-curve of the flat panel has only a moderate bend at the bifurcation point, whereas the shallow panel shows a dynamic snap-through behaviour. In the case of the deep panel the load bearing capacity decreases without a dynamic snap into a new stable configuration.

In the deep postbuckling range all three curves have positiv gradients $dN^{12}/d\gamma$. That is, curved as well as flat postbuckled panels have a load bearing capability. Nevertheless buckling causes a considerable loss in global shear stiffness. The stiffness reduction is a function of the curvature. The reduction factor increases with decreasing radius of curvature.

Figure 4 shows plots of the applied shear deformation γ versus the out-of-plane deflection u_3^ζ at the panel centre for the three panels examined. γ is normalized with respect to γ_{cr} and u_3^ζ to the panel thickness. In addition, the computed buckling modes at $\gamma/(\gamma_{cr})_{flat\,p.} = 6$ are shown. All buckling patterns have a dominant buckle running diagonally across the panel with the maximum out-of-plane deflection at the panel centre. In the case of the curved panels the dominant buckle snaps in the direction of the concave surface. With decreasing radius of curvature the buckling mode shapes change slightly. The orientation of the dominant buckle increases from 45^0 for the flat panel to approximately 60^0 for the deep one. The plotted load-central deflection curves show that no out-of-plane deflections occur below the buckling load. At the load level of the bifurcation points the deflections increase suddenly, in case of the shallow panel in form of a dynamic snap. In the deep postbuckling range the rate of increase of the deflection is a function of the panel curvature. At the same load level the flat panel has the smallest out-of-plane deflection, the deep panel the greatest. The same trend is valid for the rate of increase. In all three panels the rate of increase declines in the deep postbuckling range.

Initial geometric imperfections may have a considerable effect on the buckling behaviour of thin shell structures. Thus, it is of interest to examine the imperfection sensitivity of shear loaded curved panels. Because of its snap-through behaviour the shallow panel is chosen as example. For the computations symmetric (1-cos)-functions are used as initial imperfections. They may be regarded as approximations to the post-buckling mode of the perfect panel.

Figure 5 shows plots of the normalized angle of shear versus the out-of-plane central deflection for several imperfection amplitudes $(u_3^i)_{max}$. Applying a small imperfection amplitude ($(u_3^i)_{max} = 1\%\ t$),

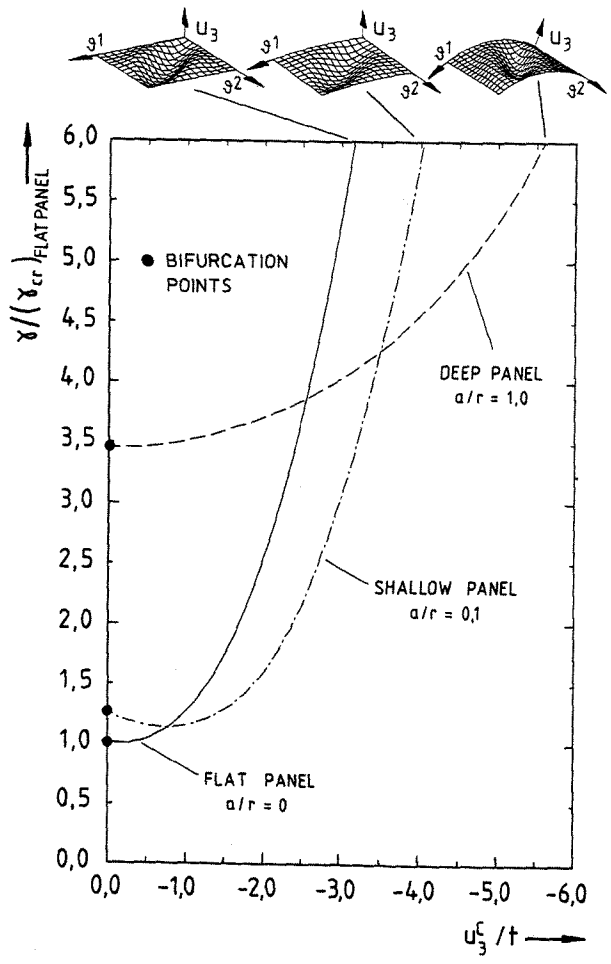

Figure 4. Effect of panel curvature on the the relation between the out-of-plane deflection u_3^ζ at the panel centre and the angle of shear γ.

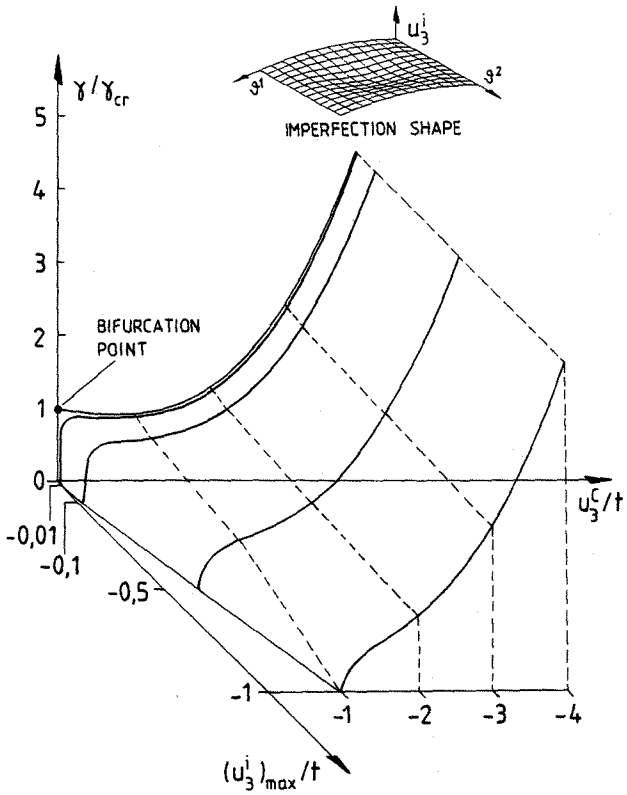

Figure 5. Effect of geometric imperfections on the relation between the out-of-plane deflection u_3^ζ at the panel centre and the angle of shear γ.

the bifurcation problem of the perfect panel ceases to exist. Instead the imperfect panel has only one nonlinear solution path but retains its snap-through behaviour. With increasing imperfection amplitudes the snap-through behaviour vanishes as well. For amplitudes greater than 10% of the panel thickness the deformation behaviour becomes nonlinear immediatly after shear loading is applied. A distinction between a pre- and post-buckling state is no longer possible. In these cases the information provided by the linear buckling load is meaningless. The influence of the geometric imperfections declines with increasing load. For an angle of shear $\gamma = 6\,\gamma_{cr}$ all load-central deflection curves are identical.

Figure 6 shows the average shear flow N^{12} versus the prescribed angle of shear γ for the studied imperfect panels. Both variables are normalized with respect to the corresponding values of the classical buckling load. The plotted curves confirm the results of Fig.5 . In the case of panels with imperfection amplitudes greater than 0,1 t the relation between the average shear flow and the angle of shear becomes nonlinear well below the bifurcation load of the perfect panel. The transition from the pre-buckling to the post-buckling state becomes smoother with increasing imperfection amplitudes.

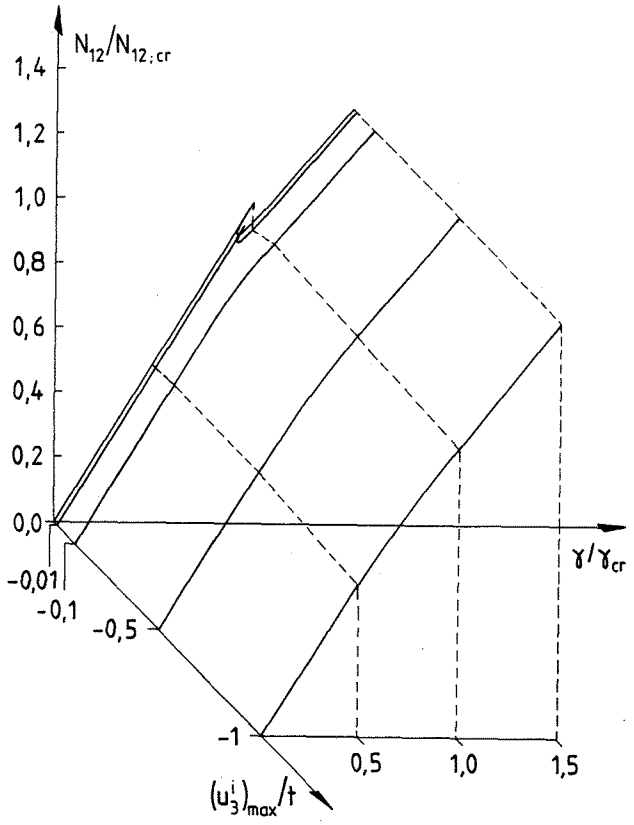

Figure 6. Effect of geometric imperfections on the relation between the average shear flow N^{12} and the angle of shear γ.

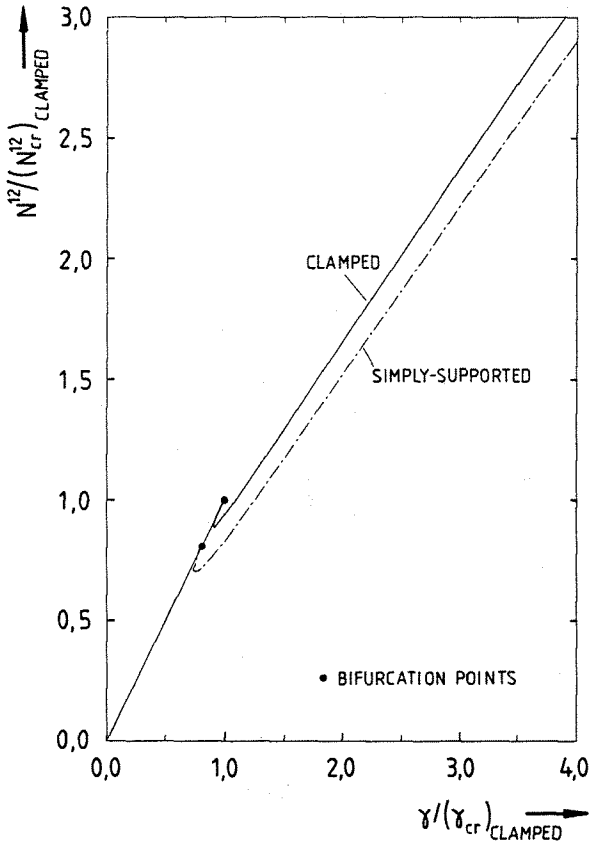

Figure 7. Effect of boundary conditions on the relation between the average shear flow N^{12} and the angle of shear γ.

The effect of different boundary conditions on the relation between the average shear flow N^{12} and the prescribed angle of shear γ is shown in Figure 7. Compared are a clamped and a simply supported shallow panel. N^{12} and γ are normalized with respect to the corresponding critical values (classical buckling load) of the clamped specimen. Both panels have a linear pre-buckling behaviour and a snap-through in in the initial postbuckling range. They differ mainly in the buckling load which is 19% lower in the case of the simply-supported panel. In the deeper postbuckling range the curves of both panels are nearly linear. The gradient of the simply-supported panel is only slightly smaller than that of the clamped one. That is, although the simply-supported edges cause a loss in load bearing capacity they have no significant influence on the shear stiffness in the deep postbuckling range.

Figure 8 shows the load-central deflection curves of the two panels. As expected, the simply-supported panel has the larger centre deflection. But the differences between the curves decrease with increasing shear loading. For example, at $\gamma/\gamma_{cr} = 8$ it has declined to 3%. Obviously the bending stiffness of the simply-sup-

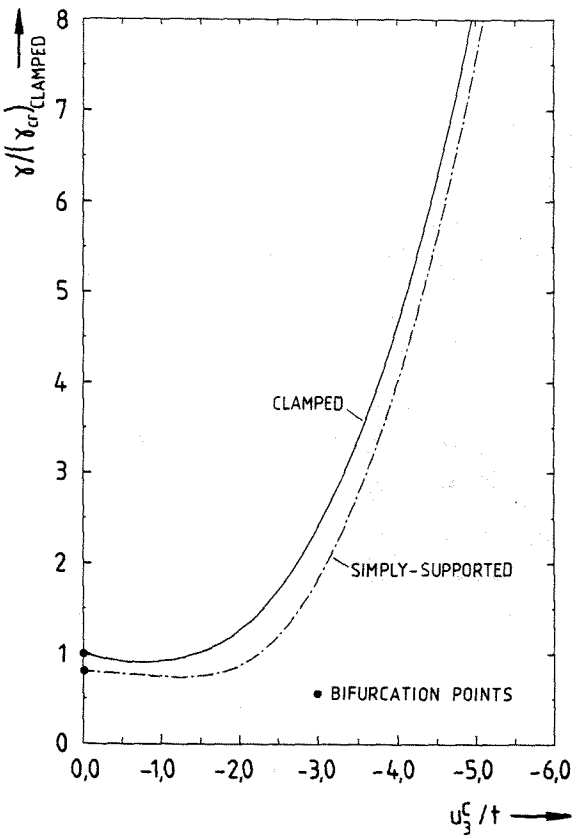

Figure 8. Effect of boundary conditions on the relation between the out-of-plane deflection u_3^{ζ} at the panel centre and the angle of shear γ.

ported edges increases in the deep post-buckling range.

Further computations yield that the influence of the boundary conditions decreases with increasing radius of curvature i.e., curved simply-supported edges behave like clamped ones.

All results presented are valid for panels having the same shape parameter $\zeta = a^2/rt$ as well as identical material properties and boundary conditions.

3. Experiments

Test specimens

Dimensions and lay-up configurations of the examined panels are listed in Table 1. The three curved specimens were identical with respect to dimensions, material and fiber-patterns. The flat panel differed only in curvature. Each test specimen consisted of eight layers of unidirectional prepreg sheets (913C/T300) and was autoclave cured with the vacuum bag technique. For manufacturing the curved panels a cylindrical shaped graphite/epoxy mold was used.

Test set-up and procedures

The test set-up used for the experimental investigations is shown in Figure 9. The tensile force applied by a Losenhausen testing machine of 200 kN capacity was transformed into a shear loading on the test panels by means of the shear frame illustrated in Fig. 9. The test specimens were bolted between four pairs of rigid steel edge members. For cylindrical panels additional fittings were used which filled the spare between the plane edge members and the curved shapes of the test specimens. The edge members were pin-jointed at their ends with the points of rotation located at the corners of the web. The frame formed a mechanism which did not contribute to the load bearing capacitiy of the system.

To determine the angle of shear of the loaded panels two inductive displacement transducers were attached to the frame which measured the elongation of the vertical (i.e., tension) and the shortening of the horizontal (i.e., compression) diagonal. The initial geometric imperfections and the buckling mode in the compression diagonal were determined by a deflection transducer which was attached to a carriage running on a slideway (see Fig. 9)

		FLAT PANEL	SHALLOW PANELS		
		P2	S2-1	S2-2	S2-3
DIMENSIONS:					
a = b	mm	400	400	} as S2-1	} as S2-1
r	mm	∞	4000		
t	mm	2,2	2,2		
t_{EXP}	mm	2,21	2,17	2,25	2,43
MATERIAL:					
resin / fibre *	-	913C/T300	} as P2	} as P2	} as P2
lay-up scheme	-	$[(45/-45)_2]_S$			
GEOM. IMP.:					
max.ampl. $(u_3^i)_{max}$	mm	-0,6	-0,45	-0,5	-0,05
mode	-	approx.symm.	as P2	as P2	as P2
CLASSICAL BUCKLING LOAD:					
γ_{cr}	deg	0,0279	0,0379	–	–
N_{cr}^{12}	N/mm	32,3	43,9	–	–

*MATERIAL PROPERTIES :

moduli : $E_1 = 116,8$ kN/mm²; $E_2 = 7,8$ kN/mm²

$G_{12} = 4,4$ kN/mm² $\nu_{12} = 0,3$

strength : $\sigma_{FT}^{11} = \sigma_{FC}^{11} = 1,54$ kN/mm²; $\sigma_F^{12} = 0,09$ kN/mm²

$\sigma_{FT}^{22} = 0,06$ kN/mm² ; $\sigma_{FC}^{22} = 0,1$ kN/mm²

Table 1. Geometric data, material properties and calculated classical buckling loads of the test panels.

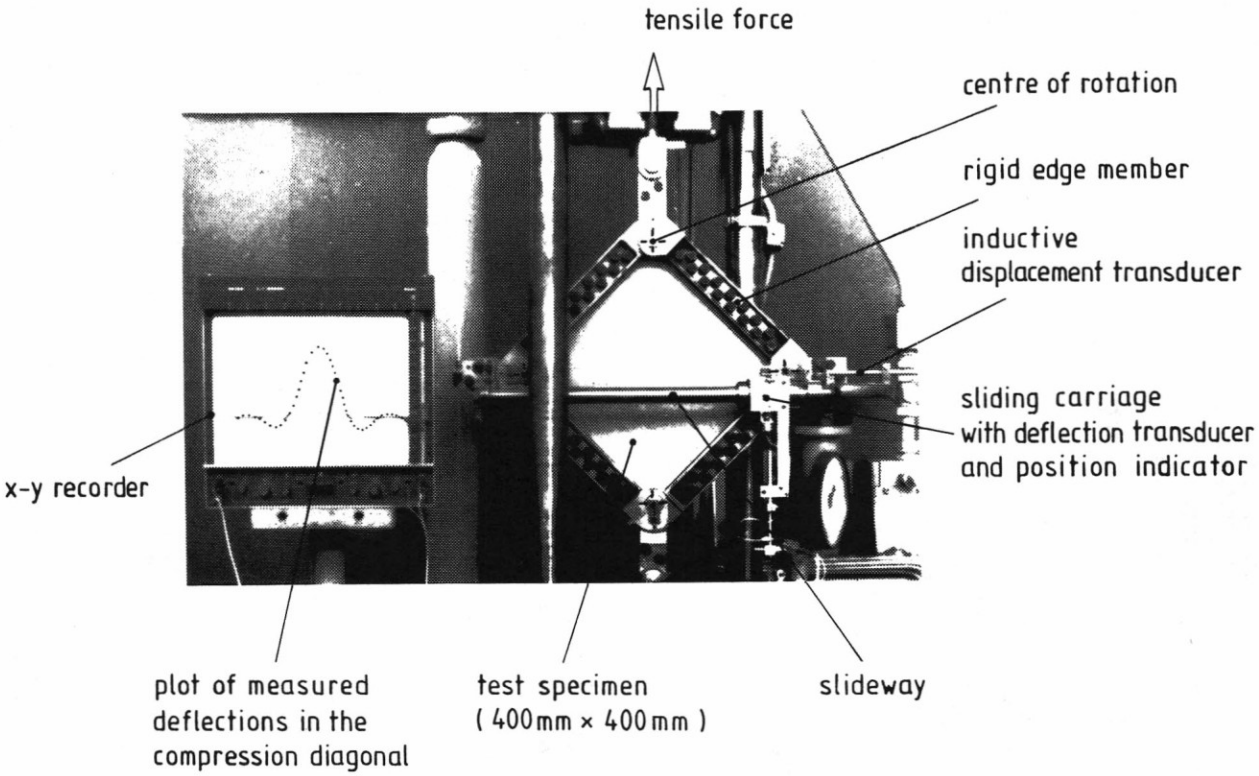

Figure 9. Test set-up.

and connected to a x-y recorder. Strain gauge rosettes positioned on both surfaces of the specimens were used to measure normal and shear strains at three points ($\vartheta^1 = \vartheta^2 = 200$ mm; $\vartheta^1 = 300$ mm, $\vartheta^2 = 200$ mm; $\vartheta^1 = \vartheta^2 = 67$ mm).

Incremental loading was applied to the shear frame until failure occured or the maximum load of the testing machine was reached. At each load increment the angle of shear, the buckling mode and the strains were determined. Prior to testing of each panel measurements of the initial geometric imperfections in the compression diagonal were conducted.

Experimental results and comparison with theoretical predictions

Some results of the experimental investigations are shown in Figures 10-13. The measured values are compared with numerical solutions. For the flat panel P2 and the shallow panel S2-1 both a classical linear buckling analysis and a geometric nonlinear analysis were performed. In addition the postbuckling behaviour of the curved panel was analysed considering the effect of material failure. A 12x12 element mesh was used for all calculations. The shear load was applied according to Fig. 2 and clamped boundary conditions were assumed. The panel dimensions and the material properties used are shown in Table 1. The initial geometric imperfections of the test specimens were approximated by symmetric (1-cos)-functions.

Figure 10 shows the measured out-of-plane centre deflections u_3^c of the four test specimens plotted versus the angle of shear γ . γ is normalized with respect to the corresponding value of the computed classical buckling load of the flat panel P2 (see Table 1). Despite the small curvature of the cylindrical panels considerable differences appear in the deformation behaviour of the flat and curved specimens. At small angles of shear the centre deflections of the curved panels increase more rapid than that of the flat one. In the deep postbuckling range the curved specimens have about 40% larger centre deflections. This tendency is in accordance with the results of the theoretical study (see Fig. 4). With the curved panels no snap-through behaviour was observed during the tests. This fact is confirmed by this figure as all specimens show a smooth transition to the postbuckling range. Therefore a defined experimental buckling load can hardly be determined. The nonlinear deformation behaviour starting from the beginning of the loading process is caused by geometric and other imperfections, as for example risidual stresses, local differences of material properties and slight asymmetries of the laminate (for the effect of geometric imperfections see Fig. 5).

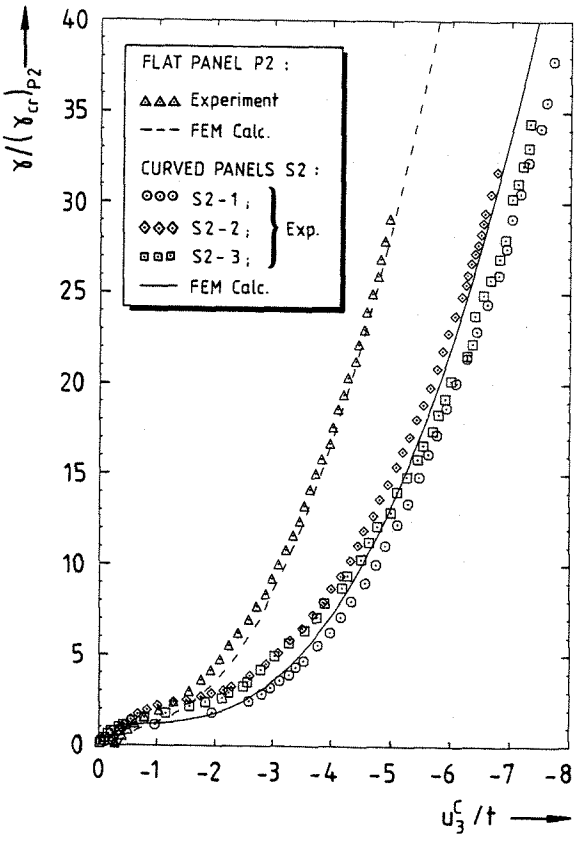

Figure 10. Measured and calculated out-of-plane deflections u_3^c at the panel centre versus the angle of shear γ .

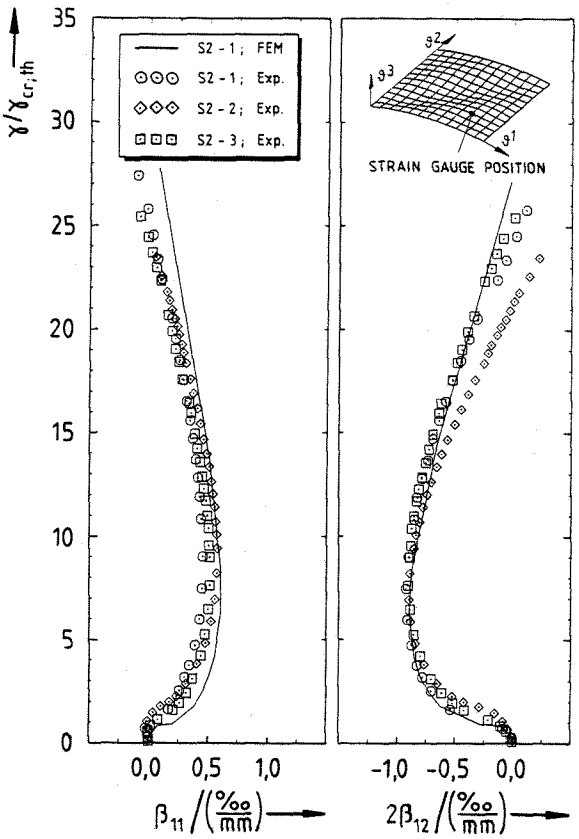

Figure 11. Measured and calculated bending strains β_{11} , β_{12} versus the angle of shear γ .

The comparison between the three curved panels yields that the greatest differences between their measured deflection curves are to be found at small angles of shear i.e., shear loads. This may be explained by the fact that these panels, although owing an identical lay-up scheme, have slightly different geometric imperfections and dimensions caused by the manufacturing process. As shown in Fig. 5, particularly the geometric imperfections have a considerable effect on the deflection behaviour in the vicinity of the theoretical buckling load. In the deep postbuckling range the differences between the test results of the three curved panels decrease.

The theoretically predicted response of P2 and S2 obtained by a geometrical nonlinear calculation is in good agreement with the test results. Local differences in deflections, especially at the beginning of the loading process, are due to the fact that the input data used for the calculations are approximations (geometric imperfections) or mean values (dimensions, material properties). Also a linear stress-strain relation of the graphit/epoxy material was assumed.

In Figure 11 the measured and calculated flexural curvatures β_{11} and β_{12} at the point $\vartheta^1 = 300$ mm; $\vartheta^2 = 100$ mm on the compression diagonal of the curved panels S2 is plotted versus the angle of shear. γ is normalized to the corresponding value of the classical buckling load. The measured strains confirm the results obtained by Fig. 10 that caused by imperfections bending occurs immediately when load is applied and therefore an experimental buckling load can hardly be determined. The calculated strain curves are in good agreement with the measured ones. Presumably the differences at high loads are caused by idealization errors in the calculation (e.g. course element mesh, assumed linear stress-strain behaviour).

In Figure 12 theoretical results obtained from a geometric nonlinear analysis and a nonlinear computation considering the effect of material failure are compared to the test results for the panel S2-1. The figure shows the centre deflections u_3^c versus the angle of shear γ . u_3^c is normalized to the panel thickness and γ to the corresponding value of the classical buckling load. The nonlinear failure analysis yields a first ply failure (FPF) well above the theoretical buckling load ($\gamma = 8{,}7\ \gamma_{cr}$). This first ply failure is a matrix failure in the top ply at the tension corners. At $\gamma = 15{,}8\ \gamma_{cr}$ the first fibre failure occurs. The comparison of the two calculated deflection

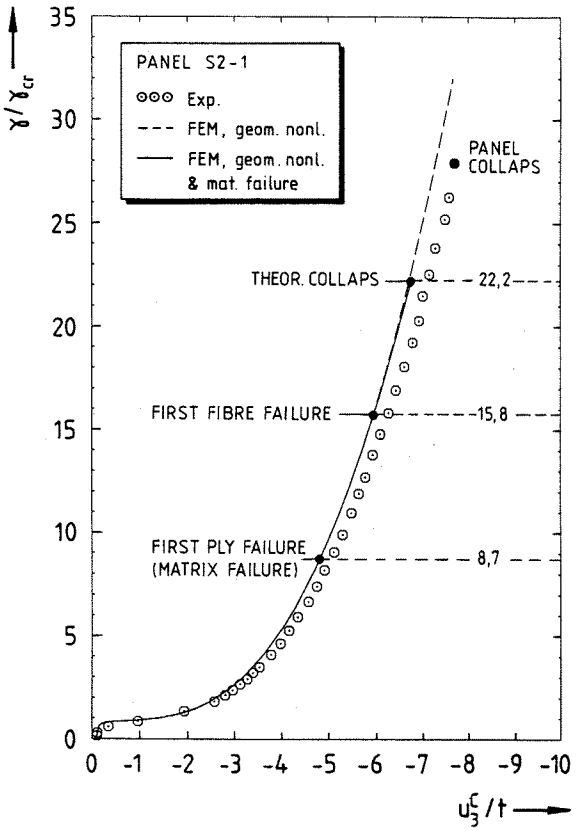

Figure 12. Out-of-plane deflections u_3^{ζ} at the panel centre versus the angle of shear γ (spec. S2-1); predicted failure loads.

curves shows that neither matrix nor fibre failures have a considerable effect on the deflection behaviour of the panel. Only at high load levels the deflection increases slightly. This predicted response is in accordance with the experimental results. The measured deflection curve shows no significant discontinuities or changes in increase. The predicted collapse of the panel occurs at 80% of the experimentally obtained angle of shear. This difference is due to several factors, such as material imperfections, the effect of the used element mesh on the "smeared crack" area and the reliability of the used failure criterias. Nevertheless the theoretical result may be regarded as a good estimation.

In Figure 13 the calculated damage zones at the theoretical collaps load are depicted for the 8 layers of the panel. The figure shows that material failure occurs mainly in areas with maximum curvature. Matrix failure happens mainly in the -45° layers in which the global tension load acts normal to the fibres. Fibre breakage is limited to the corners of the tension diagonal. The comparison with the test specimen reveals that the positions of fibre failure are in good agreement with the location of the crack leading to the panel collapse.

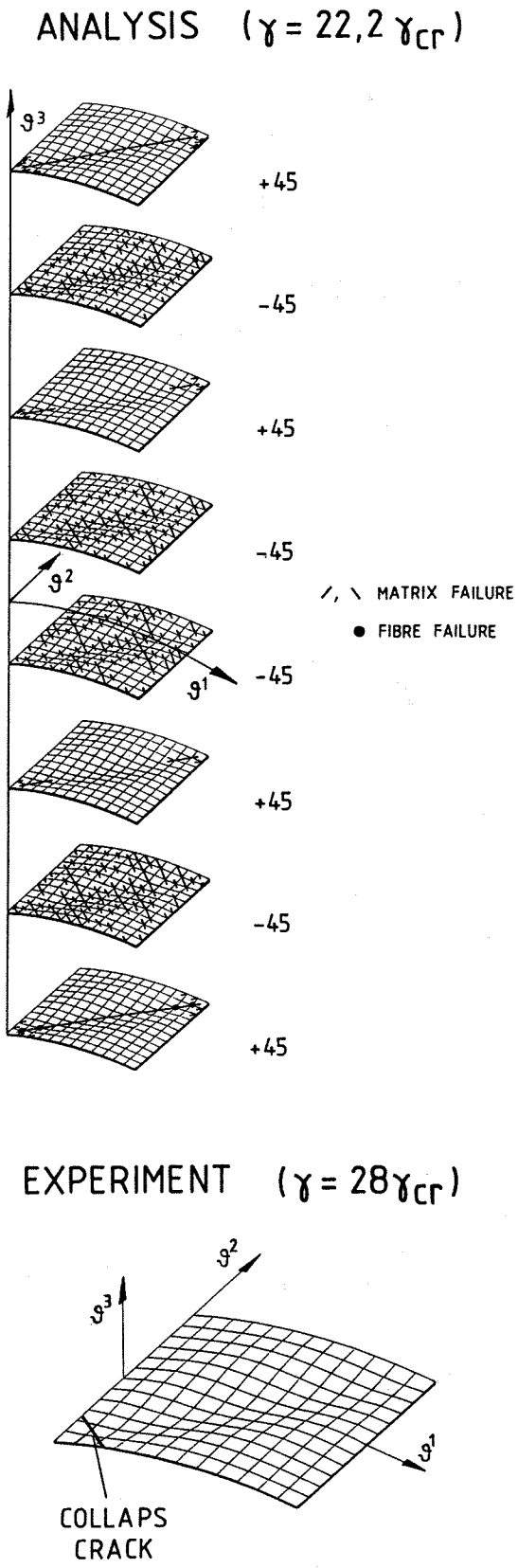

Figure 13. Predicted damage zones at the theoretical collaps load of specimen S2-1.

4. Conclusion

The buckling and postbuckling behaviour of curved carbon fibre reinforced plastic shear panels was examined both theoretically and experimentally.

After developing a mixed finite element computer program, linear buckling loads and nonlinear postbuckling paths were computed for some cylindrical panel configurations. From these examples the following conclusions may be summarized:

Curved shear loaded CFRP panels as well as composite plates have a load bearing capability in the postbuckled state. The buckling load as well as the initial and the deep postbuckling behaviour are influenced mainly by the panel curvature. With decreasing radius of curvature the buckling load (i.e., bifurcation load) increases, whereas the global shear stiffness decreases in the deep postbuckling range. Identical shear deformation assumed, curved panels have larger out-of-plane deflections than flat ones.

Initial geometric imperfections result in a nonlinear panel response starting immediately when the shear load is applied. With increasing shear loading the effect of initial imperfections on the postbuckling behaviour declines.

Perfect simply-supported curved panels have lower bifurcation loads than clamped ones. The differences in the postbuckling behaviour between clamped and simply-supported panels decrease with increasing shear loading.

In order to verify the theoretical results, flat and shallow cylindrical CFRP panels were tested. The experiments confirmed that curved postbuckled panels have a considerable load carrying capacity and larger out-of-plane deflections than identical flat panels. The nonlinear load-deformation behaviour of the test specimens was analysed using the developed numerical method. The computed deformations, strains and failure maps showed a good correlation with the experimental results. The comparison verified the ability of the computer program to predict the nonlinear buckling behaviour of curved laminated shear panels with reasonable accuracy.

Acknowledgement

The research effort leading to the results presented herein was financially supported by the "Deutsche Forschungsgemeinschaft". This support is gratefully acknowledged.

References

(1) KOBAYASHI,S.; SUMIHARA.K.; KOYAMA,K.: "Compressive Buckling Strength of Graphit-Epoxy Laminated Curved Panels", in: Proc. of the 15th ICAS-Congress, London, Sept. 1986, pp.244-254

(2) KUDVA,N.J.; AGARWAL,B.L.: "Postbuckling Analysis of Stiffened Composite Shear Panels - Theoretical Analysis and Comparison with Experiments", in: Proc. of the 102nd ASME-Winter Meeting, Washington D.C., Nov. 1981, pp. 221-229

(3) TUNKER,H.: "Über das Tragverhalten schubbeanspruchter quadratischer Platten aus Faserverbundwerkstoffen bei großen Deformationen", Diss., Techn. Universität Braunschweig, 1982

(4) PALAZOTTO,A.N.; STRAW,A.D.: "Shear Buckling of Cylindrical Composite Panels", Comp. & Struct. 27 (1987), pp. 689-692

(5) HUI,D.; DU,I.H.Y.: "Imperfection-Sensitivity of Long Antisymmetric Cross-Ply Cylindrical Panels under Shear Loads", J. Appl. Mechanics (1987), pp. 292-298

(6) WILKINS,D.J.; OLSON,F.: "Shear Buckling of Advanced Composite Curved Panels", Experimental Mechanics 14 (1974), pp. 326-330

(7) KRÖPLIN,B.-H.: "Postbuckling Instability Analysis of Shells Using the Mixed Method", in: Buckling of Shells, Springer Verlag, Berlin-Heidelberg-New York-Tokyo, 1982

(8) BATHE,K.-J.: "Finite-Elemente-Methoden", Springer Verlag, Berlin-Heidelberg-New York-Tokyo, 1986

(9) WASHIZU, K.: "Variational Methods in Elasticity and Plasticity", 3rd ed., Pergamon Press, Oxford, 1982

(10) BASAR,Y.; KRÄTZIG,W.B.: "Mechanik der Flächentragwerke", Vieweg Verlag, Braunschweig-Wiesbaden, 1985

(11) TSAI,S.W.; HAHN,H.T.: "Introduction to Composite Materials", Technomic Publishing Company, Westport, 1980

(12) RAMM,E.: "The Displacement Finite Element Method in Nonlinear Buckling Analysis of Shells", in: Buckling of Shells, Springer-Verlag, Berlin-Heidelberg-New York, 1982

(13) WOLF,K.; KOSSIRA,H.: "Zur Berechnung des nichtlinearen Tragverhaltens von Strukturen aus Faserverbundwerkstoffen", in: Entwicklung und Anwendung von Faserverbund-Strukturen, DGLR-Bericht 87-02, Bonn, 1987

(14) "Bruchhypothesen und Reservefaktoren (Grundlagen)", in: Luftfahrttechnisches Handbuch / Band Faserverbund-Leichtbau, VB 33300-03, 1983